Acta Pharmaceutica Sinica B 2024;14(6):2505–2519

Chinese Pharmaceutical Association
Institute of Materia Medica, Chinese Academy of Medical Sciences

Acta Pharmaceutica Sinica B

www.elsevier.com/locate/apsb
www.sciencedirect.com

ORIGINAL ARTICLE

Ciclopirox inhibits SARS-CoV-2 replication by promoting the degradation of the nucleocapsid protein

Xiafei Wei[a,†], Yuzheng Zhou[a,†], Xiaotong Shen[a,†], Lujie Fan[b,†], Donglan Liu[c,†], Xiang Gao[a], Jian Zhou[a], Yezi Wu[a], Yunfei Li[a], Wei Feng[a], Zheng Zhang[a,*]

[a]*Institute for Hepatology, National Clinical Research Center for Infectious Disease, Shenzhen Third People's Hospital, Southern University of Science and Technology, Shenzhen 518112, China*
[b]*Guangzhou Laboratory, Guangzhou Medical University, Guangzhou 511495, China*
[c]*State Key Laboratory of Respiratory Disease, National Clinical Research Center for Respiratory Disease, Guangzhou Institute of Respiratory Health, the First Affiliated Hospital of Guangzhou Medical University, Guangzhou 510120, China*

Received 9 December 2023; received in revised form 4 February 2024; accepted 28 February 2024

KEY WORDS

SARS-CoV-2;
Nucleocapsid protein;
Viral replication;
Ciclopirox;
Abnormal aggregation;
Protein degradation;
Autophagy–lysosome;
Drug target

Abstract The nucleocapsid protein (NP) plays a crucial role in SARS-CoV-2 replication and is the most abundant structural protein with a long half-life. Despite its vital role in severe acute respiratory syndrome coronavirus 2 (SARS-CoV-2) assembly and host inflammatory response, it remains an unexplored target for drug development. In this study, we identified a small-molecule compound (ciclopirox) that promotes NP degradation using an FDA-approved library and a drug-screening cell model. Ciclopirox significantly inhibited SARS-CoV-2 replication both *in vitro* and *in vivo* by inducing NP degradation. Ciclopirox induced abnormal NP aggregation through indirect interaction, leading to the formation of condensates with higher viscosity and lower mobility. These condensates were subsequently degraded *via* the autophagy-lysosomal pathway, ultimately resulting in a shortened NP half-life and reduced NP expression. Our results suggest that NP is a potential drug target, and that ciclopirox holds substantial promise for further development to combat SARS-CoV-2 replication.

*Corresponding author.
E-mail address: zhangzheng1975@aliyun.com (Zheng Zhang).
†These authors made equal contributions to this work.
Peer review under the responsibility of Chinese Pharmaceutical Association and Institute of Materia Medica, Chinese Academy of Medical Sciences.

https://doi.org/10.1016/j.apsb.2024.03.009

1. Introduction

As the coronavirus disease 2019 (COVID-19) pandemic caused by SARS-CoV-2 enters its fourth year, more than 700 million cases have been reported, resulting in over 6.9 million deaths[1]. Although multiple vaccines and drugs are currently being approved[2,3], the public health threat posed by the virus remains significant, mainly because of its rapid mutation[4]. Therefore, it is crucial to develop new potential targets and drugs to establish a foundation for the prevention and control of new mutant strains and emerging infectious diseases.

SARS-CoV-2 is a positive-sense RNA virus with a genome length of approximately 30 kb. It encodes four structural proteins: the spike, envelope, membrane, and nucleocapsid proteins[5]. Among these proteins, nucleocapsid protein (NP) is highly expressed in infected cells and conserved across various SARS-CoV-2 strains[6]. The NP consists of two domains: the N-terminal domain (NTD) and the C-terminal domain (CTD)[7]. The NTD binds to RNA for genome packaging, whereas the CTD facilitates NP dimerization for capsid assembly[8,9]. Additionally, NP interacts with host proteins and plays a role in multiple inflammatory responses and immune-regulatory processes[10]. Previous studies have reported that NP activates the inflammatory signaling pathway, disrupts the innate immune response, and contributes to the development of a cytokine storm or "long COVID"[11-13]. Therefore, reducing NP expression can considerably attenuate the viral replication capacity and lung inflammatory response. Considering the critical role of NP in SARS-CoV-2 replication, it is a crucial target for drug development. Based on virtual screening, several studies have identified small molecular compounds targeting NP, such as K31[14], arbidol, ceftriaxone[15], and phenanthridine derivatives[16], which specifically interfere with the interaction between the NTD and viral genomic RNA. Other studies have reported compounds that disrupt the phase separation of NP, such as 1,6-hexanediol[17], GCG[18], PJ34, and CV218[19]. Additionally, certain inhibitors, including alectinib, which targets SRPK1/2[20], and lithium, which targets GSK-3, have been found to decrease viral propagation by suppressing NP phosphorylation[21].

Despite the discovery of inhibitors that interfere with the normal physiological functions of NP, no NP inhibitors have been approved for clinical use. This is mainly because the binding pocket between the NP and the inhibitor is structurally highly dynamic, hindering the stability of the inhibitor binding to the NP. Moreover, NP wraps intricately with viral RNA and folds into a ribonucleoprotein complex, leading to a lower drug binding efficiency[22]. Furthermore, we previously found that NP exhibited unusual stability with a super-long half-life of at least 48 h (Supporting Information Fig. S1A and S1B). However, no small-molecule compounds that promote NP degradation have been reported. Therefore, given the difficulties in developing functional NP inhibitors and the high-abundance signature caused by the super-long half-life of NP, this study aimed to identify small-molecule compounds that promote NP degradation.

Ciclopirox is an antifungal agent[23], with anticancer and antiviral effects[24]. Ciclopirox strongly inhibits the replication of HSV1 and HSV2. Ciclopirox blocks the enzymatic activity of the nucleotidyl transferase superfamily, which is essential for HSV replication[25,26]. Several studies have reported that ciclopirox effectively inhibits HIV replication. Ciclopirox acts as a DOHH inhibitor by interfering with the hypusination modification of eIF5A, ultimately causing an HIV maturation disorder[27,28]. Moreover, ciclopirox inhibits HBV replication by binding to the core dimer−dimer interface to disrupt HBV capsid assembly[29]. In the present study, we found that ciclopirox markedly suppressed SARS-CoV-2 replication, both *in vitro* and *in vivo*. Mechanistically, ciclopirox induced NP to form abnormal condensates, which were then degraded *via* the autophagy−lysosomal pathway. Our findings suggested that NP might serve as a potent antiviral target and the NP inhibitor, ciclopirox, might be a promising drug for inhibiting SARS-CoV-2 replication.

2. Materials and methods

2.1. Cell lines and cell culture

HEK293T, Vero-E6, HeLa-ACE2, and HeLa-NP cells were cultured in Dulbecco's modified Eagle's medium (11,960,044, Gibco, Grand Island, USA) supplemented with 10% fetal bovine serum (FBS, 10,099,158, Gibco). Calu-3 cells were maintained in MEM (11,090,081, Gibco) supplemented with 20% FBS. HeLa-ACE2 cells expressing human ACE2 were generated *via* transduction with an ACE2-expressing lentiviral vector. HeLa-NP cells expressing the SARS-CoV-2 NP were generated by transduction with an NP-expressing lentiviral vector.

2.2. Compound preparation and cell viability assay

An FDA-approved compound library was purchased from MCE (HY-L022, MCE, NJ, USA). Ciclopirox was obtained from the MCE for *in vitro* and *in vivo* experiments. Ferrous sulfate was obtained from the Sigma (PHR1483, Merk KGaA, Darmstadt, Germany). Cell viability was measured using a cell counting kit 8 (C0037, Beyotime, Shanghai, China). The 50% maximal effect concentration (EC_{50}) and 50% cytotoxic concentration (CC_{50}) values were calculated using GraphPad Prism software (version 6.0).

2.3. SARS-CoV-2 virus preparation and infection

The SARS-CoV-2 WT, delta, and Omicron strains were isolated from nasopharyngeal aspirate specimens sourced from COVID-19 patients in SHENZHEN Third People's Hospital. The virus was expanded in Vero-E6 cells and stored at −80 °C. When performing viral infection experiments, Calu-3 and HeLa-ACE2 cells were usually infected with an MOI of 0.5 for 1 h at 37 °C, while Vero-E6 with an MOI of 0.05. All experiments involving SARS-CoV-2 infection were performed in the Biosafety Level 3 laboratory of SHENZHEN Third People's Hospital, following standard operating procedures.

2.4. Viral titers assay

The viral titers of SARS-CoV-2 were determined using a focus-forming assay (FFA). Briefly, cell supernatants were collected after treatment with the compound, and virus were collected and serial dilutions of the supernatants were transferred into a 96-well plate seeded with Vero-E6 cells at 37 °C for 1 h. The inocula were removed and fresh medium containing carboxymethylcellulose (419,273, Sigma) was added. After 24 h, the plates were fixed with 4% paraformaldehyde (E672002, Sangon, Shanghai, China) for 30 min and permeabilized with 0.1% TritionX-100 (85,111, Thermo Fisher Scientific, Waltham, MA, USA) for 30 min. Horseradish peroxidase (HRP)-conjugated anti-SARS-CoV-2 nucleocapsid antibody (40,143-R040-H, Sino Biological, Beijing, China) was added to the plates and incubated for 2 h at room temperature. The plates were washed with PBS and incubated with True Blue peroxidase substrate (5510-0030, Seracare Life Sciences, USA) for approximately 10 min at room temperature. SARS-CoV-2 titers were calculated using an ELISpot system (Cytation 7, Bio-Tek, Vermont, USA). Viral titers were calculated as FFU per mL.

2.5. RNA extraction and quantitative RT-PCR

Total RNA was extracted from cells or animal lungs using TRIzol reagent (DP424, TIANGEN, Beijing, China) following the manufacturer's instruction. The RNA was transcribed into cDNA using the FastKing cDNA kit (KR118, TIANGEN). Quantitative analysis of the target genes was performed through quantitative reverse transcription polymerase chain reaction (RT-qPCR) using the SYBR Green qPCR Kit (FP205, TIANGEN). The primer sequences used are listed in the Supporting InformationTable S1.

2.6. Animal experiments

The 6−8 weeks old BALB/C mice were intranasally transduced with 2.5×10^8 FFU AD5-hACE2. Seven days later, the mice were anesthetized and intranasally inoculated with the WT SARS-CoV-2 strain. The SARS-CoV-2-infected mice were treated with 20 mg/kg/day ciclopirox or dimethyl sulfoxide (DMSO) diluted in 60% propylene glycol and 30% physiological saline for 5 days. Subsequently, the mice body weights were monitored daily until they were sacrificed at the end of the experiment. Their lungs were then harvested to assess viral titers, RT-qPCR, hematoxylin and eosin (H&E) staining, and immunofluorescence staining. Animal experiments involving authentic SARS-CoV-2 were conducted at the Guangzhou Customs District Technology Center ABSL-3 Laboratory. The experimental animal procedures used in this study were approved by the Institutional Animal Care and Use Committee of the Affiliated First Hospital of Guangzhou Medical University (No. 20230058).

2.7. Immunohistochemical (IHC) assay

IHC assays were performed previously described[30]. Tissue sections were stained with H&E to assess pathological changes and were subsequently stained with primary anti-SARS-CoV-2 NP (1:400; AB2827975, Sino Biological) and secondary antibodies to test for SARS-CoV-2 antigen expression.

2.8. Western blotting

Cells were lysed with RIPA buffer (P0013C, Beyotime), and the lysates were centrifuged at 13,000 rpm for 15 min (Eppendorf 5424R). The supernatants were collected and mixed with the loading buffer for 10 min. Subsequently, samples were separated using sodium dodecyl sulfate-polyacrylamide gel electrophoresis, followed by blotting onto PVDF membranes. The membranes were blocked with milk and then incubated using the following primary antibodies: anti-SARS-CoV-2 NP (1:3000, AB2827975, Sino Biological), anti-SARS-CoV-2 spike (1:1000, 40,591-R235, Sino Biological), anti-HA (1:1000, MA1-12429, Thermo Fisher Scientific), anti-Strep (1:2000, MA5-17283, Thermo Fisher Scientific), anti-His (1:1000, MA1-21315, Thermo Fisher Scientific), anti-GAPDH (1:3000, 10,094-MM13, Sino Biological), and anti-β-actin (1:3000, AF0003, Beyotime). Afterward, the membranes were incubated with HRP-conjugated anti-IgG (1:5000, HS101, TransGen Biotech, Beijing, China) and detected using a chemiluminescence detection ECL kit (32,106, Thermo Fisher Scientific) and a ChemiDoc Imaging system (ChemiDocMP, BIO-RAD, California, USA). The results were quantified using the ImageJ software.

2.9. His-Ub pull-down assay

HEK293T cells were seeded into 6-well plates at 80%−90% density. The cells were transfected with the plasmid His-Ub or vector and harvested using 8 mol/L urea lysis buffer (8 mol/L urea, 500 mmol/L NaCl, 10 mmol/L imidazole, 10 mmol/L Tris-HCl pH 8.0, 10% glycerol, and 0.1% Triton X-100) on ice for 1 h. The cell lysate was centrifuged at 12,000×g for 10 min (Centrifuge 5424R, Eppendorf, Hamburg, Germany), and the supernatants were incubated with Ni-NTA agarose (600,442, Thermo Fisher Scientific) and rotated for 2 h at 4 °C. The agarose was washed approximately four times with the urea lysis buffer. Subsequently, the samples were eluted with buffer (0.15 mol/L Tris-HCl pH 6.7, 200 mmol/L imidazole, 5% SDS, 0.72 mol/L β-ME, and 30% glycerol) and then subjected to Western blot analysis.

2.10. Confocal immunofluorescence microscopy and fluorescence recovery after photobleaching assay

For the immunofluorescence assay, HeLa cells cultured on glass coverslips were transfected with the NP-GFP plasmid or infected with SARS-CoV-2. The cells were fixed with 4% paraformaldehyde for 30 min, permeabilized with 0.3% Triton X-100, and blocked with 5% BSA. The infected cells were incubated with the appropriate primary: for NP, 1:400 (AB2827975, Sino Biological); for Spike, 1:200 (40,591-R235, Sino Biological); for LAMP1, 1:40 (9091, CST, Massachusetts, USA); for LC3B, 1:50 (L7543, Sigma) and secondary antibodies (Alexa Fluor, Thermo Fisher Scientific) and washed with PBS. After counterstaining the nuclei with DAPI (5 μg/mL, C1002, Beyotime), the slides were examined under a fluorescence confocal microscope (LSM 980, Zeiss, Jena, Germany).

Furthermore, the fluorescence recovery after photobleaching (FRAP) assay was conducted at the live cell level using a Zeiss 980 fluorescence confocal microscope with a 63× oil immersion objective. The NP spots induced by ciclopirox or poly(I:C) were photobleached with 100% laser power using a 488 nm laser, and time-lapse images were captured after bleaching. The recovery of fluorescence intensity from photobleaching was recorded in an Excel table at the indicated time points. Excel data were processed using ImageJ and Graphpad Prism6.0.

2.11. Cellular thermal shift assay

The cellular thermal shift assay (CETSA) assay was performed as previously described[31]. For cell lysate CETSA, cells expressing NP were seeded into a 24-well plate and harvested using trypsin solution. The cell precipitates dissolved in 1 mL PBS buffer (containing 1 g/L glucose, 0.5% DMSO, and 1 × cocktail protease inhibitor) were lysed by freeze-thawing four times through liquid nitrogen and centrifuged at 13,000 rpm for 10 min at 4 °C (Eppendorf 5424R). Equal amounts of supernatant were distributed into PCR tubes and incubated with ciclopirox or DMSO for 30 min at room temperature. The mixture was heated with a gradient from 45 to 55 °C in a PCR thermocycler for approximately 3 min and then cooled on ice for 5 min. The soluble and insoluble proteins were separated by centrifugation at 13,000 rpm for 30 min (Eppendorf 5424R). Soluble proteins were collected and analyzed using Western blotting.

For the intact cell CETSA, the cells expressing NP were treated with ciclopirox or DMSO for 3 h at 37 °C. Drug-treated cells were harvested and resuspended in PBS, and equal amounts of the suspension were placed in PCR tubes. The samples were

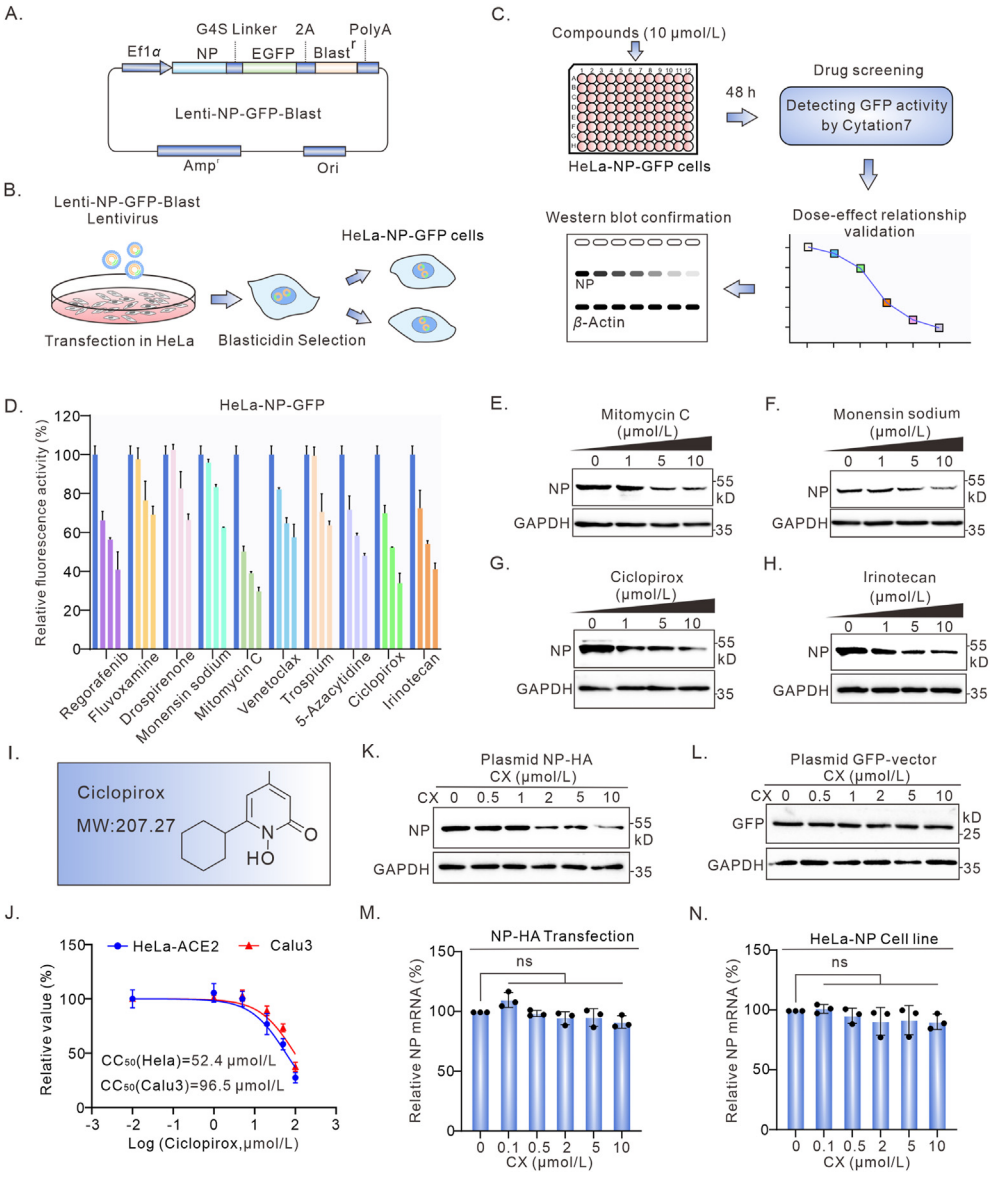

Figure 1 Identification of small molecule compounds that promoted NP degradation from FDA-approved library. (A) Diagram of the Lenti-NP-GFP-Blast plasmid. (B) Construction of an NP-GFP stable cell line using a lentiviral system. (C) The strategy of the compound screening system for identifying NP inhibitors. (D) HeLa-NP-GFP cells were treated with compounds (the concentrations were 0, 1, 5, and 10 μmol/L) for 48 h. The cells were fixed with 4% paraformaldehyde and then incubated with DAPI. The signal ratio GFP/DAPI was scanned and calculated using Cytation 7 ($n = 3$). (E−H) The HeLa-NP cells were treated with compounds for 48 h. The cells were collected and the NP/GAPDH protein level was detected by Western blotting. (I) The chemical structure of ciclopirox. (J) HeLa and Calu3 cells were treated with ciclopirox to determine the CC_{50} using the CCK8 agent ($n = 3$). (K, L) HeLa cells were transfected with plasmid NP-HA or vector GFP for 8 h, and then the cells were treated with ciclopirox for 48 h. The protein samples were analyzed using Western blotting. (M, N) The mRNA levels of NP-HA plasmid-transfected or HeLa-NP cells were treated with ciclopirox for 48 h. The RNA was extracted with TRIzol and determined through RT-qPCR. Statistical significance was determined using the one-way ANOVA, "ns" indicates no significant difference. Data are presented as mean ± SD, $n = 3$.

then heated using a thermocycler and lysed four times in liquid nitrogen by freeze-thawing. The soluble proteins were separated and detected as described above.

2.12. The half-life assays

For the half-life assay of NP protein, the cells expressing NP were seeded into 24-well plates and allowed to reach approximately 90%−100% confluence. The cells were treated with different concentrations of ciclopirox or DMSO for 48 h and then treated with the protein synthesis inhibitor-cycloheximide (CHX, HY-12320, MCE) (100 μg/mL). The cells were harvested at the indicated time points and analyzed using Western blotting.

For the half-life assay of NP mRNA, the cells expressing NP were seeded into a 12-well plate for 24 h. The cells were treated with DMSO/ciclopirox and actinomycin D (HY-17559, MCE) (0.5 μg/mL). The RNA was harvested by TRIzol agent at the indicated time points and analyzed by RT-qPCR.

2.13. Surface plasmon resonance (SPR) assay

The SARS-CoV-2 Nucleocapsid protein (40588-V07E15, Sino Biological) was directly immobilized through amine coupling on the CM5 chip using the SPR instrument (Biacore 8K, Cytiva, Uppsala, Sweden), and the sample was used as the analyte. Diluting the analyte to the different concentrations by the running buffer and then performing kinetic detection. Biacore 8K Software v.3.0.12.15655 was used for binding studies.

2.14. Isothermal titration calorimetry (ITC)

The binding assay of ciclopirox to NP was performed by an ITC instrument (PEAQ-ITC, MicroCal, Massachusetts, USA) at 25 °C. The ciclopirox and NP (40,588-V07E15, Sino Biological) were dissolved in assay buffer (20 mmol/L Tris pH 8.0, 20 mmol/L NaCl, 0.2% DMSO). 200 μmol/L of ciclopirox in the syringe was injected into the sample cell containing 20 μmol/L of NP solution. Data was determined by the MicroCal PEAQ-ITC analysis software to obtain ΔH, ΔS, and K_D values.

2.15. Statistical analysis

All experiments were repeated at least three times and all results in the figures are presented as the mean ± SD. Unpaired Student's *t*-test, one-way ANOVA, and two-way ANOVA were performed using GraphPad Prism 6. Differences were considered statistically significant when $P < 0.05$ (*), $P < 0.01$ (**), $P < 0.001$ (***), and $P < 0.0001$ (****).

3. Results

3.1. Identification of small molecule compounds that promoted NP degradation from FDA-approved compounds

To screen for small molecule compounds that promote NP degradation, we first engineered a cell model to screen drugs targeting NP. An NP-GFP plasmid containing a GFP tag fused to the C-terminus of NP was constructed (Fig. 1A). This plasmid was integrated into HeLa cells by lentiviral packaging and the cell line was named HeLa-NP-GFP (Fig. 1B). As shown in Fig. 1C, these compounds underwent screening and validation. The FDA compound library containing 1800 compounds was tested in the first screening using the HeLa-NP-GFP cell line. Approximately 47 compounds with a 1.5-fold decrease in the GFP signal were selected for drug dose-effect validation. 10 out of the 47 compounds induced a dose-dependent response of GFP activity in HeLa-NP-GFP cells (Fig. 1D). These 10 compounds were tested in HeLa-NP cells for their ability to reduce NP expression. Four compounds (mitomycin C, monensin sodium, ciclopirox, and irinotecan) caused a dose-dependent reduction in NP expression (Fig. 1E−H). The CC_{50} of the four compounds was evaluated in HeLa cells. The CCK8 results showed that ciclopirox had a higher CC_{50}, while the other three compounds had lower CC_{50} (Supporting Information Fig. S1C−S1F). Thus, we prioritized ciclopirox for further study.

The chemical structure of ciclopirox is shown in Fig. 1I. The CC_{50} of ciclopirox in HeLa-ACE2 and Calu3 cells was 52.4 and 96.5 μmol/L, respectively (Fig. 1J). Ciclopirox treatment caused a dose-dependent NP reduction in a transiently transfected NP system (Fig. 1K) but did not reduce GFP or mCherry expression in a GFP or mCherry transiently transfected system (Fig. 1L and Fig. S1G). Immunofluorescence results also showed that ciclopirox specifically reduced the NP expression, but did not affect the expression of GFP and mCherry (Fig. S1H). We further evaluated the effects of ciclopirox on the expression of other structural and non-structural proteins of SARS-CoV-2. The Western blot results revealed that ciclopirox did not reduce the expression levels of other structural and non-structural proteins except for NP (Fig. S1I−S1U), indicating that the ability of ciclopirox to reduce NP expression was specific.

To analyze how ciclopirox reduced the expression level of NP, we first examined the effect of ciclopirox on the transcription level of NP. As shown in Fig. 1M and N, ciclopirox did not inhibit the synthesis of NP mRNA during either transient transfection or stable expression of NP. Additionally, we also examined whether ciclopirox degraded NP mRNA. After treatment with actinomycin D (RNA synthesis inhibitor), the effect of ciclopirox on the half-life of NP mRNA was detected at the indicated time points. The RT-qPCR results showed that compared with DMSO treatment, ciclopirox treatment could not accelerate the degradation of NP mRNA (Fig. S1V). These results suggested that ciclopirox inhibited NP expression mainly at the protein level rather than at the transcriptional level.

3.2. Ciclopirox induced an abnormal NP aggregation by indirectly interacting with NP

Since the expression of NP was very strong during both transient transfection and stable expression, this might partially mask the efficacy of ciclopirox. To further determine whether ciclopirox promoted NP degradation, we generated a cell line expressing tetracycline/doxycycline-inducible NP expression (HeLa-TRE-NP-tTA) (Supporting Information Fig. S2A). The doxycycline treatment increased intracellular NP levels in a dose-dependent manner (Fig. 2A). In this cell line, ciclopirox potently induced NP degradation, and this phenomenon was most prominent at low NP expression level (Fig. 2B−D). Consistent with the above results, we also demonstrated that ciclopirox did not affect the degradation rate of NP mRNA using the HeLa-TRE-NP-tTA cell line (Fig. S2B). To study the mechanism by which ciclopirox induced NP degradation, the interaction between ciclopirox and NP was analyzed using CETSA. First, the NP thermal stability was assessed using CETSA. The NP was denatured at different

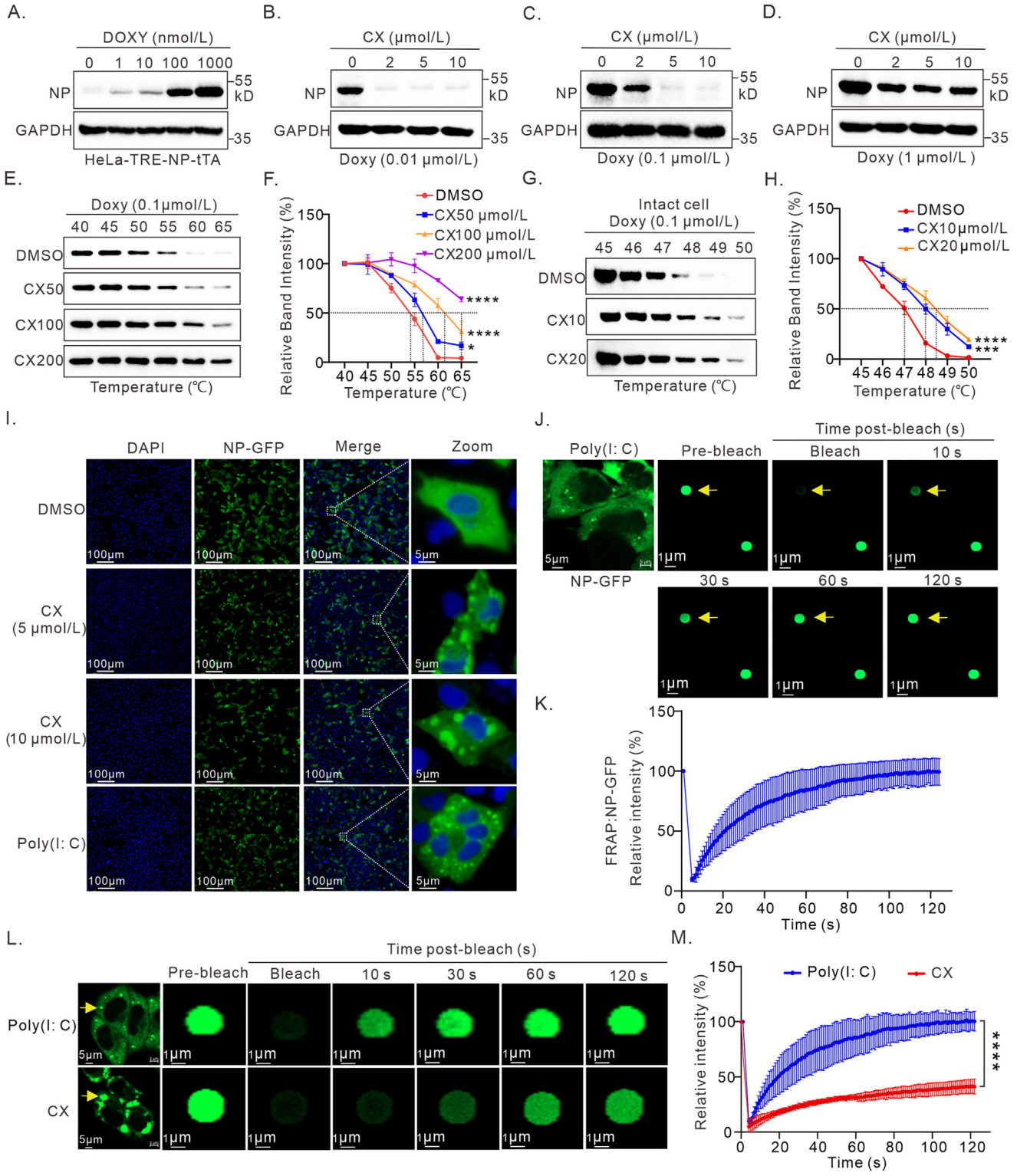

Figure 2 Ciclopirox induced an abnormal aggregation of NP by indirectly interacting with NP. (A−D) HeLa-TRE-NP-tTA cells were treated with doxycycline or ciclopirox for 48 h. Protein levels were determined using Western blotting. (E, F) HeLa-TRE-NP-tTA cells were treated with 0.1 μmol/L doxycycline for 24 h. The cells were lysed with liquid nitrogen and protein samples were collected and incubated with ciclopirox or DMSO for the CETSA. CETSA results are shown through Western blotting. Gray values were calculated using ImageJ software. (G, H) HeLa-TRE-NP-tTA cells were first treated with 0.1 μmol/L doxycycline for 24 h and then incubated with ciclopirox for 3 h. The cells were heated and lysed for CETSA. In (F) and (H), data are presented as mean ± SD, $n = 3$. (I) HeLa cells were transfected with NP-GFP plasmid. 8 h later, the cells were treated with different concentrations (0, 5, and 10 μmol/L) of ciclopirox for another 48 h or transfected with poly(I:C) for 6 h. The cells were immunostained. Scale bar, 100 μm. Expanded views are also shown. (J, K) HeLa cells expressing the NP-GFP protein were stimulated by

temperatures. The results revealed that the NP thermal stability exhibited a good gradient trend when it was at an interval temperature of 40−65 °C (Fig. S2C). Under these conditions, the cell lysate CETSA was performed to study the interaction between ciclopirox and the NP. The NP showed temperature-induced unfolding, with a mean melting temperature (T_m) of 54 °C. The addition of ciclopirox increased the Tm of NP in a dose-dependent manner (Fig. 2E and F) but did not alter the Tm of GAPDH (Fig. S2D and S2E). These results were similar to the CETSA results obtained using intact cell samples (Fig. 2G−H,Fig. S2F and S2G). These findings suggested that ciclopirox interacted with NP to disrupt NP thermal stability. To further explore whether ciclopirox was directly bound to NP, the SPR assay was performed. However, the SPR result showed no direct interaction between ciclopirox and NP (Fig. S2H). Additionally, the ITC result also showed no direct interaction between ciclopirox and NP (Fig. S2I and S2J). These results revealed that ciclopirox disrupted NP function by indirectly interacting with NP.

Consistent with previous reports, the NP was mainly localized in the cytoplasm in a diffuse manner[8]. Interestingly, compared to the DMSO treatment group, ciclopirox treatment induced NP aggregation and the formation of punctate condensates. Additionally, the number and size of punctate condensates gradually increased with increasing ciclopirox concentration (Fig. 2I). Multiple teams have previously reported that the liquid−liquid phase separation (LLPS) of SARS-CoV-2 NP contributes to viral replication and assembly[32]. To evaluate whether SARS-CoV-2 NP undergoes LLPS in cells, we transfected the plasmid NP-GFP into HeLa cells and observed that NP formed droplets in the cytoplasm after poly(I:C) stimulation. Furthermore, the NP-enriched droplets readily underwent efficient diffusion and recovered quickly following the FRAP assay (Fig. 2J and K). To explore the differences between ciclopirox-induced NP condensates and poly(I:C)-induced NP droplets, we analyzed the fluorescence recovery time after the FRAP assay. FRAP results established that poly(I:C)-induced NP droplets were highly dynamic, with 90%−100% fluorescence recovery within 2 min of photobleaching. However, the ciclopirox-induced NP condensates exhibited much higher viscosity, with only 30%−50% fluorescence recovery (Fig. 2L and M). This suggested that ciclopirox induced abnormal NP aggregation to form condensates with increased viscosity and decreased mobility, which was usually accompanied by reduced solubility. Furthermore, these abnormal NP condensates were more likely to be degraded and removed by cellular protein quality control systems.

3.3. *The ciclopirox-induced NP condensates were degraded via the autophagy−lysosomal pathway*

As ciclopirox did not affect the NP mRNA level, it may regulate NP protein stability. To test this hypothesis, we performed a chase assay to evaluate the effect of ciclopirox on the protein level of NP. Western blotting showed that the half-life of NP treated with DMSO was greater than 48 h, whereas the half-life of NP treated with ciclopirox was significantly shortened (Fig. 3A and B). This indicated that ciclopirox degraded NP by attenuating its stability.

Previous studies have shown that aggregated proteins are primarily degraded by the autophagy−lysosomal system[33,34]. To investigate the pathway involved in ciclopirox-induced NP degradation, we treated cells with the proteasome inhibitors MG132 and bortezomib (Borte) or lysosomal inhibitors, such as bafilomycin A1 (BafA1) and 3-methyladenine (3-MA) in the presence or absence of ciclopirox. In the ciclopirox-untreated group, neither proteasome nor lysosomal inhibitors affected the NP protein expression levels. Nevertheless, in the ciclopirox-treated group, BafA1, and 3-MA, but not proteasome inhibitors mostly rescued ciclopirox-induced NP degradation (Fig. 3C and D). Additionally, we explored whether ciclopirox degraded NP in a ubiquitin-mediated manner. The ubiquitin pull-down assays revealed that after MG132 treatment, the ciclopirox-induced NP reduction still led to a diminished level of NP ubiquitination (Fig. 3E). In contrast, after 3-MA treatment, ciclopirox-induced NP degradation was significantly reversed and the NP ubiquitination level was restored to some extent (Fig. 3F). This indicated that ciclopirox did not increase the NP ubiquitination after treatment with either MG132 or 3-MA. Furthermore, immunofluorescence assay demonstrated that co-treatment with ciclopirox and the lysosomal inhibitor 3-MA led to a pronounced accumulation of NP condensates, whereas no such accumulation was observed in cells treated with ciclopirox and the proteasome inhibitor MG132, indicating that ciclopirox-induced NP degradation occurred through the ubiquitin-independent lysosomal pathway (Fig. 3G).

Next, to determine whether ciclopirox induced the co-localization between NP and lysosome, immunofluorescence experiments were performed. The results revealed that ciclopirox induced the co-localization between NP condensates and the lysosome-associated membrane protein 1 (LAMP1, a lysosome marker). After BafA1 treatment, the volume and quantity of ciclopirox-induced NP condensates were increased, and the co-localized signal between NP condensates and lysosome became stronger (Fig. 3H). Finally, to analyze whether ciclopirox induced autophagic degradation of NP, we performed an immunostaining assay. The results showed that ciclopirox treatment induced the NP condensates to co-localize with LC3B protein (the autophagosome marker). In contrast, the NP droplets induced by poly(I:C) stimulation did not co-localize with LC3B (Fig. 3I). These results collectively supported the hypothesis that ciclopirox-induced NP condensates were degraded *via* the autophagy−lysosomal pathway.

3.4. *Ciclopirox inhibited SARS-CoV-2 replication at a post-entry step*

To investigate whether ciclopirox effectively inhibited SARS-CoV-2 replication, we performed experiments on three cell lines. We first evaluated the CC_{50} and EC_{50} of ciclopirox against the viral RNA. The ciclopirox CC_{50} for Calu3, HeLa-ACE2, and Vero-E6 cells was 104.7, 47.2, and 44.9 μmol/L, respectively. The ciclopirox EC_{50} against viral RNA for Calu3, HeLa-ACE2, and Vero-E6 cells was 2.8, 1.7, and 1.3 μmol/L, respectively (Fig. 4A−D, and G). Next, we examined the effects of ciclopirox

poly(I:C) for 8 h, and then performed the FRAP assay. Scale bar, 5 μm. Expanded views are also shown. (L, M) HeLa cells expressing the NP-GFP protein were incubated with 10 μmol/L ciclopirox or 1 μg/mL poly(I:C) for 24 h and subjected to FRAP assay. Scale bar, 5 μm. Expanded views are also shown. Statistical significance was calculated using the two-way ANOVA. *$P < 0.05$, ***$P < 0.001$, and ****$P < 0.0001$. In (K) and (M), data are presented as mean ± SD, $n = 6$.

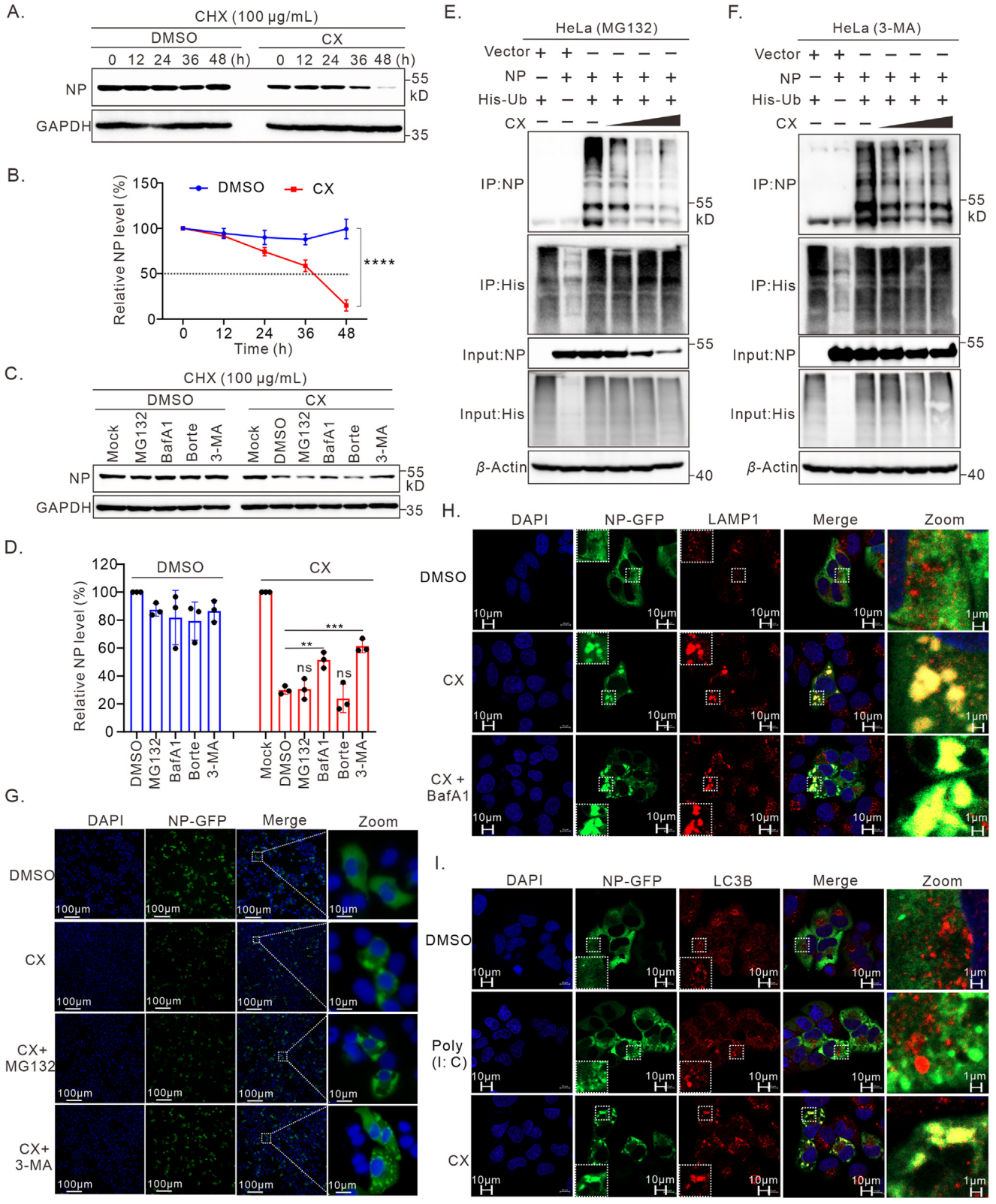

Figure 3 The Ciclopirox-induced NP condensates were degraded *via* the autophagy lysosomal pathway. (A) HeLa-NP cells were treated with DMSO or 5 μmol/L ciclopirox for 48 h. After 100 μg/mL CHX treatment, the protein samples were harvested at the indicated time, and the NP protein levels were determined by Western blotting. (B) NP quantification using Western blotting is shown as relative percentages. $^{****}P < 0.0001$, by the two-way ANOVA, $n = 3$. (C, D) The HeLa-NP cells were treated with DMSO or 5 μmol/L ciclopirox for 48 h, followed by treatment with 10 μmol/L MG132, 500 nmol/L BafA1, 5 μmol/L bortezomib, or 10 mmol/L 3-MA for another 8 h. The cells were lysed and subjected to Western blotting. The NP levels are presented as percentages. The error bars indicated the mean ± SD, $n = 3$. $^{**}P < 0.01$,

on other SARS-CoV-2 indicators using Western blotting and IF assays. Western blotting showed that ciclopirox significantly inhibited the levels of NP and spike protein (Fig. 4B, C, E, F, H, and I). The IF assay showed that ciclopirox treatment reduced the expression of spike protein (Fig. 4J). More importantly, ciclopirox treatment caused a dose-dependent decrease in NP and induced NP aggregation to form condensates in the SARS-CoV-2 infected cells (Fig. 4K).

Next, we investigated the stage of SARS-CoV-2 replication that was affected by ciclopirox. First, the ciclopirox antiviral potency was assessed using a time of addition assay (Fig. 5A). Viral RNA and protein levels were determined using RT-qPCR and western blotting, respectively. The results showed that ciclopirox treatment during SARS-CoV-2 inoculation did not inhibit the viral mRNA and protein levels, confirming that ciclopirox did not affect SARS-CoV-2 infection. However, ciclopirox treatment before and after viral infection strongly inhibited SARS-CoV-2 replication, indicating that ciclopirox mainly played a role in the post-entry step (Fig. 5B−G). To further verify this conclusion, cells were incubated with ciclopirox or diltiazem (a small molecule compound that has been reported to inhibit the early step of SARS-CoV-2 infection[35]) for 1 h, and then infected with SARS-CoV-2. The levels of viral RNA were determined at 1, 2, and 6 h post-infection using RT-qPCR. The results showed that diltiazem treatment decreased the viral RNA level as early as 1 h post-infection, whereas ciclopirox treatment only slightly decreased the level of viral RNA at 6 h post-infection, which indicated that ciclopirox did not inhibit the early step of SARS-CoV-2 infection (Supporting Information Fig. S3A).

Next, we evaluated whether ciclopirox could combat the various SARS-CoV-2 variants. Western blotting and viral titer assays revealed that ciclopirox inhibited the WT (Fig. 5H−J), Omicron (Fig. 5K−M), and Delta (Fig. 5N−P) variants in the cell lysates and supernatants. This suggested that ciclopirox might acted as a broad-spectrum inhibitor to against SARS-CoV-2 variants.

3.5. *Ciclopirox attenuated SARS-CoV-2 replication and ameliorated lung pathology in the SARS-CoV-2 infected mouse model*

To determine whether ciclopirox inhibited SARS-CoV-2 replication *in vivo*, an animal assay was performed using a BALB/C-hACE2 mouse model. BALB/C mice (6−8 weeks old) were first transduced with AD5-hACE2. Seven days later, the mice were intranasally infected with SARS-CoV-2. Simultaneously, the mice were intraperitoneally injected with 20 mg/kg ciclopirox or DMSO for five consecutive days (Fig. 6A). In the DMSO-treated group, infected mice showed reduced vitality and dull fur after two days. Furthermore, the body weight of the DMSO-treated mice was reduced by approximately 10%, while the ciclopirox-treated mice showed a distinct improvement in body weight (Fig. 6B).

Ciclopirox treatment significantly reduced SARS-CoV-2 titers and viral gene expression in lung tissues (Fig. 6C and D). Furthermore, IHC staining of the SARS-CoV-2 protein in the lung tissue showed that ciclopirox significantly reduced viral protein expression, which was consistent with the results of viral indicators described previously (Fig. 6E). Lung tissues were collected for H&E staining to assess the pathological changes. Compared to the non-infected mock group, the lungs of the DMSO-treated group showed extensive infiltration of interstitial inflammatory and endothelial cells into the alveolar space, alveolar structure collapse, and alveolar hemorrhage. In contrast, the lungs of the ciclopirox-treated group showed attenuated pathological damage. After ciclopirox treatment, the infiltration of inflammatory and endothelial cells in the alveolar space of the mouse lungs was markedly reduced. Moreover, the ciclopirox-treated group showed mild hemorrhage and an intact alveolar structure (Fig. 6F). Given that ciclopirox reduced pulmonary inflammatory lesions, we detected the expression level of cytokines and pro-inflammatory factors in the lung tissues. The RT-qPCR results showed that the ciclopirox treatment reduced the mRNA levels of *Ifn-γ*, *Il-1β*, *Tnf*, *Cxcl9*, and *Cxcl10* in the infected mice, which suggested that ciclopirox exhibited anti-inflammatory ability (Fig. 6G−K). Collectively, these results confirmed that ciclopirox significantly inhibited SARS-CoV-2 replication and ameliorated lung pathology *in vivo*.

4. Discussion

The present study demonstrated that ciclopirox, an FDA-approved drug, significantly inhibited SARS-CoV-2 replication *in vitro* and *in vivo*. Mechanistically, CETSA, SPR, and ITC experiments confirmed an indirect interaction between ciclopirox and NP. Immunofluorescence results revealed that ciclopirox promoted abnormal NP aggregation. FRAP experiments indicated that the ciclopirox-induced NP condensates exhibited distinct protein physiological properties. Unlike the liquid droplets formed by the NP phase separation, the NP condensates induced by ciclopirox exhibited higher viscosity and reduced mobility. Furthermore, Chase assays revealed that ciclopirox promoted NP degradation by shortening its protein half-life. Immunostaining results confirmed that the ciclopirox-induced NP condensates were co-localized with LAMP1 and LC3B, which suggested that the degradation of ciclopirox-induced NP condensates was mediated through the autophagy−lysosomal pathway. Finally, *in vitro* and *in vivo* experiments confirmed that ciclopirox effectively inhibited SARS-CoV-2 replication by inducing NP degradation.

***$P < 0.001$, by one-way ANOVA. (E, F) NP-Strep plasmid was transfected into HEK293T cells with or without the His-Ub plasmid for 8 h. The cells were treated with ciclopirox or DMSO for 48 h and then incubated with MG132 or 3-MA for another 8 h. The NP ubiquitination was analyzed with the His pull-down assay using Ni-NTA agarose and the protein was determined through Western blotting using indicated antibodies. (G) The HeLa cells transfected with plasmid NP-GFP were treated with DMSO or ciclopirox for 48 h. Subsequently, the cells were incubated with MG132 or 3-MA for 8 h. The cells were fixed and immunostained. Scale bar, 100 μm. (H) The HeLa cells expressing the NP-GFP protein were seeded into a 35 mm glass bottom dish and then treated with DMSO or ciclopirox for 24 h, followed by treatment with 500 nmol/L BafA1 for 8 h. The cells were immunostained for DAPI (blue), NP (green), and LAMP1 (red). Scale bar, 10 μm. Expanded views were also shown. (I) The HeLa cells expressing the NP-GFP protein were treated with DMSO, poly(I:C), or ciclopirox for 24 h. The cells were immunostained. Confocal micrographs showed DAPI (blue), NP (green), and LC3B (red). Scale bar, 10 μm. Expanded views are also shown.

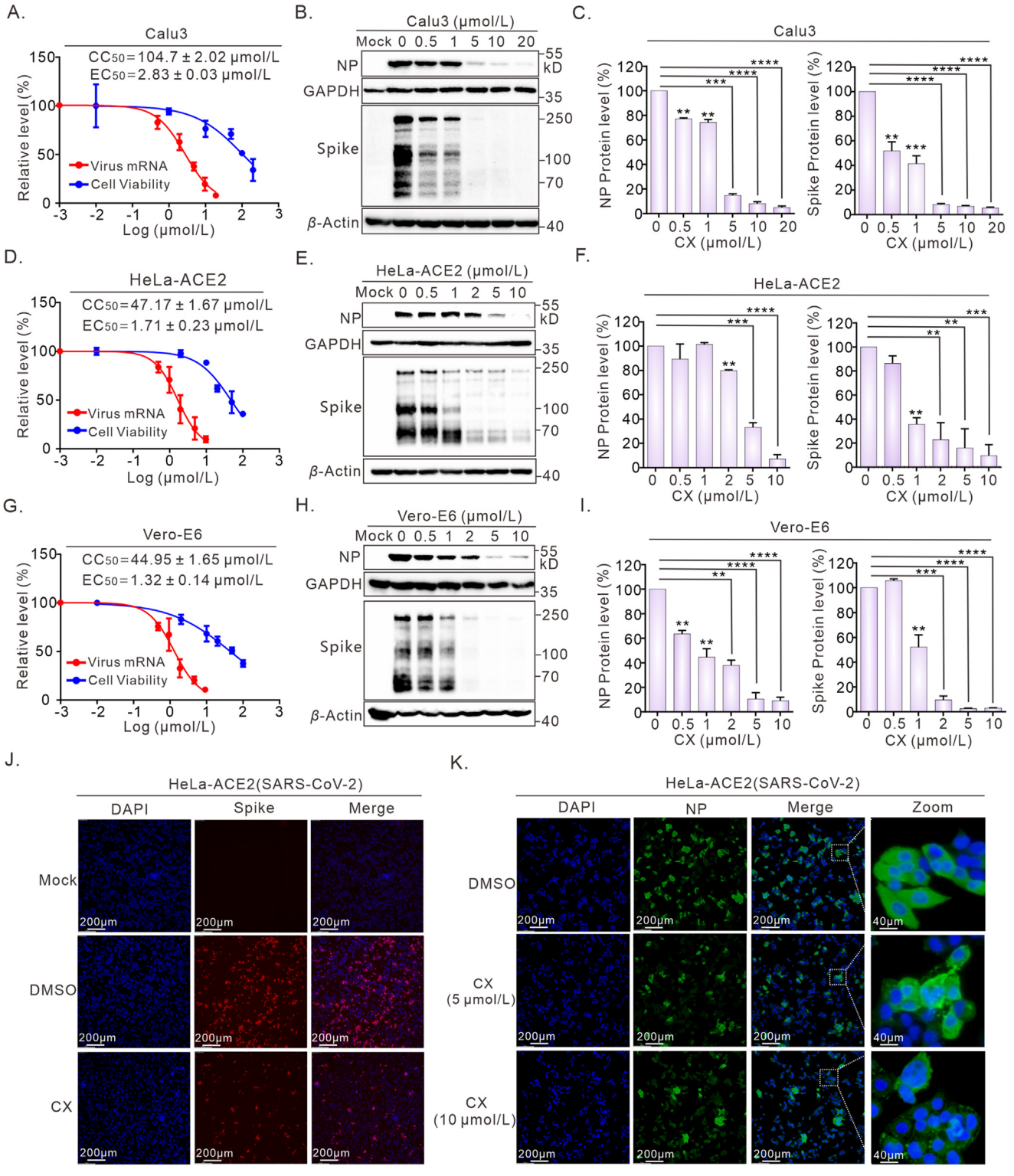

Figure 4 Ciclopirox inhibited SARS-CoV-2 replication in multiple cell lines. (A, D, G) Cells treated with DMSO or ciclopirox at the indicated concentrations were infected with SARS-CoV-2 (MOI = 0.5 for Calu3 and HeLa-ACE2; MOI = 0.05 for Vero-E6). Cell viability was determined using the CCK8 reagent. Total RNA was extracted 24 h post-infection and viral RNA levels were determined through RT-qPCR. Data are presented as mean ± SD, $n = 3$. (B, C, E, F, H, I) The infected cells were lysed with RIPA buffer at 24 h post-infection, and the protein levels of NP and spike protein were determined by Western blotting. In (C, F, I), data are presented as mean ± SD, $n = 3$. Statistical significance was calculated using the one-way ANOVA, $^{**}P < 0.01$, $^{***}P < 0.001$ and $^{****}P < 0.0001$. (J, K) The HeLa-ACE2 cells treated with DMSO or ciclopirox were infected with SARS-CoV-2 (MOI = 0.5). The cells were fixed and immunostained for spike protein (red), NP (green), and DAPI (blue). Scale bar, 200 μm.

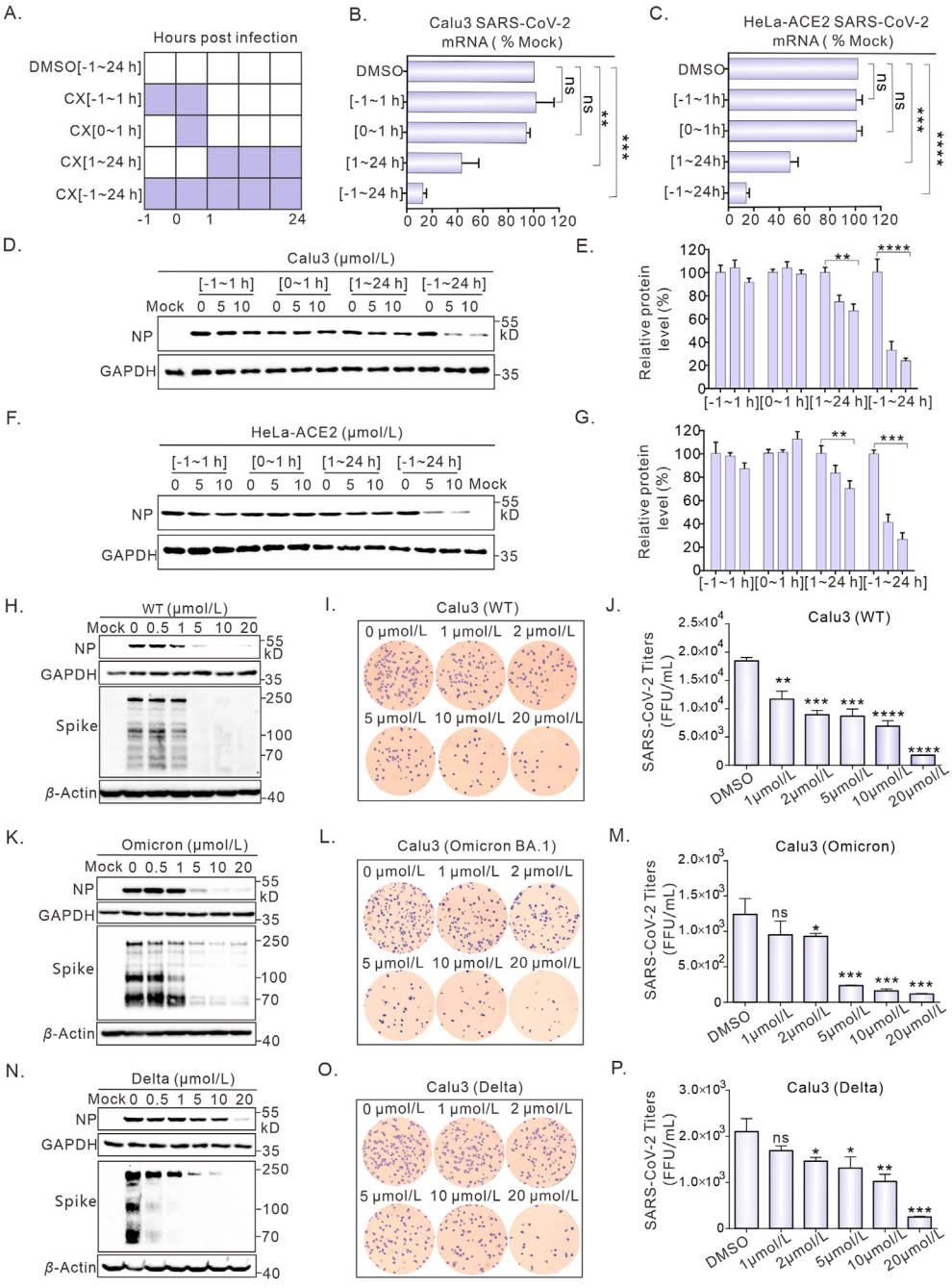

Figure 5 Ciclopirox inhibited SARS-CoV-2 replication at a post-entry step. (A) SARS-CoV-2 infected Calu3 and HeLa-ACE2 cells were treated with ciclopirox in a time of addition assay. (B, C) At 24 hpi, total RNA was extracted and viral mRNA levels were determined by RT-qPCR. Data are presented as mean ± SD, $n = 3$. (D−G) Cell lysates were harvested at 24 hpi to detect viral proteins by Western blotting ($n = 3$). (H, K, N) The levels of NP and spike protein were analyzed by Western blotting in SARS-CoV-2 variants (WT, Delta, and Omicron) infected Calu3 cells. (I, J, L, M, O, P), viral titers were determined with the FFU assay. In (J, M, P), data are presented as mean ± SD, $n = 3$. Statistical significance was calculated using the one-way ANOVA, "ns", no significant, $^{*}P < 0.05$, $^{**}P < 0.01$, $^{***}P < 0.001$, $^{****}P < 0.0001$.

As a crucial component of SARS-CoV-2, NP participates not only in the viral RNA packaging process but also in the regulation of inflammatory and immune responses[10]. Wu et al.[17] demonstrated that SARS-CoV-2 exploits the LLPS property of NP to recruit TAK1 and IKKβ into the RNA-NP aggregates, thereby hyperactivating the NF-κB pathway. Pan et al.[36] discovered that NP interacts with NLRP3, promoting inflammasome assembly and leading to cytokines overexpression, which ultimately causes acute lung inflammation and damage. Therefore, NP degradation can significantly inhibit viral replication and suppress inflammatory storms. Our findings are similar to those of previous studies, as we confirmed that ciclopirox not only inhibited viral replication in infected mice but also effectively ameliorated lung pathology. Furthermore, the infiltration of the immune cells and the expression of inflammatory signaling factors were notably suppressed. There are two possible explanations for this phenomenon. Firstly, ciclopirox-induced NP degradation weakened the inflammatory response caused by NP itself. Secondly, ciclopirox exerted anti-

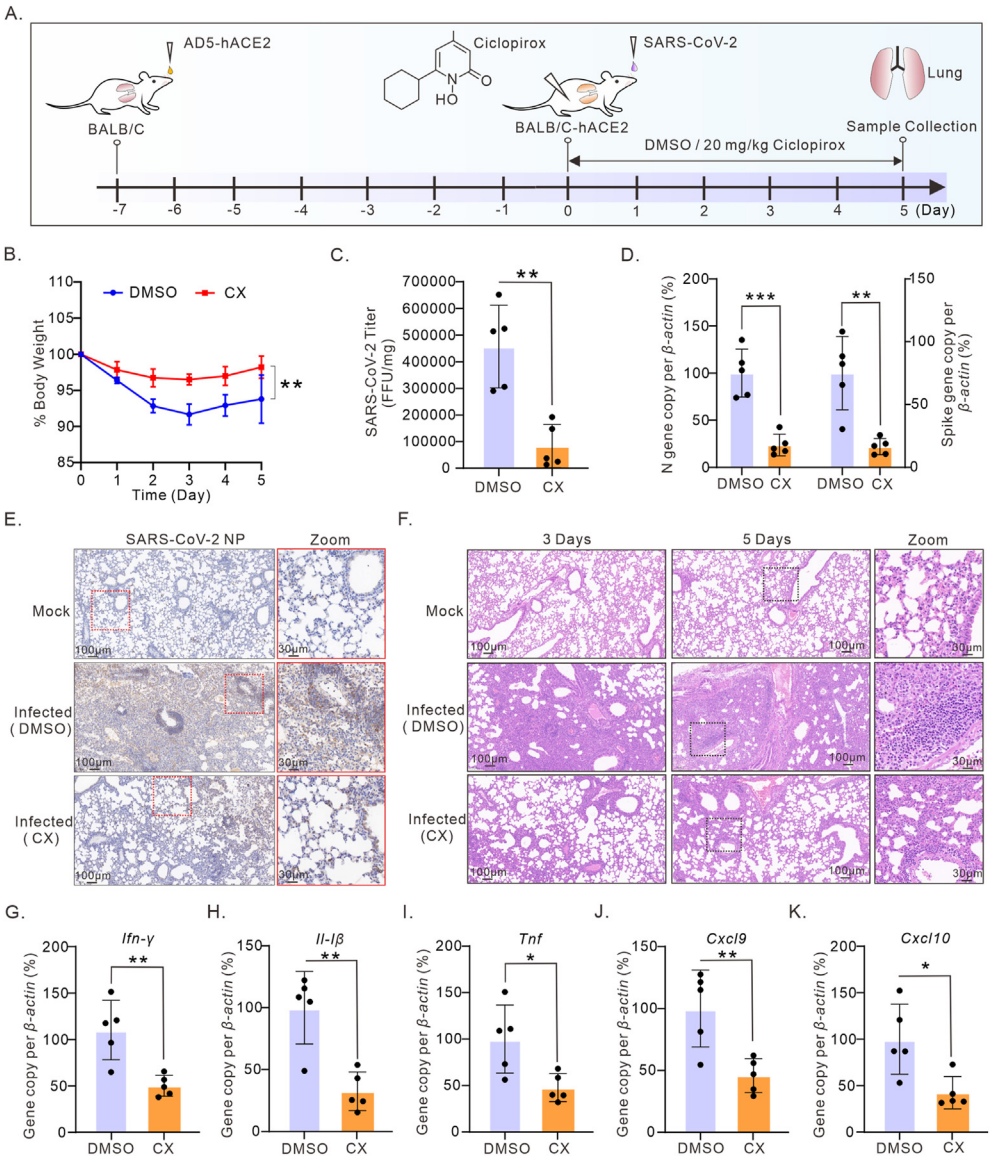

Figure 6 Ciclopirox attenuated SARS-CoV-2 replication and ameliorated lung pathology in the SARS-CoV-2-infected mouse model. (A) BALB/C-hACE2 mice were intranasally inoculated with SARS-CoV-2 and intraperitoneally administered 20 mg/kg/day ciclopirox or DMSO for five days. (B) Mice Body weights were recorded post-infection from Day 0 to Day 5. Statistical significance was calculated using the two-way ANOVA, $^{**}P < 0.01$, data are presented as mean ± SD, $n = 5$. (C, D) SARS-CoV-2 titers and viral mRNA levels in infected mice were measured by the FFA assay and RT-qPCR ($n = 5$). (E) Expression of SARS-CoV-2 NP in infected mouse lungs treated with ciclopirox or DMSO was evaluated through immunofluorescence staining with an NP antibody. Scale bar, 100 μm. (F) Representative images of H&E staining of the lungs of the infected mice. Scale bar, 100 μm. (G−K) The lungs of mice in each group were evaluated for the expression of cytokines and chemokines using RT-qPCR. Data are presented as mean ± SD, $n = 5$. Statistical significance was calculated using the unpaired Student's *t*-test, $^{*}P < 0.05$, $^{**}P < 0.01$, $^{***}P < 0.001$.

inflammatory ability. Previous studies have found that ciclopirox inhibits the activation of NLRP3 inflammasome and regulates the PGC-1α expression to reduce the production of mitochondrial ROS. In this case, the mitochondrial biosynthesis was enhanced while IL-1β release was reduced, ultimately inhibiting the inflammatory response[37]. Moreover, eIF5A hypusination has been reported to play an important role in the mRNA translation of inflammatory genes. Ciclopirox, acting as a DOHH inhibitor, might reduce the translation of inflammatory factors by disrupting the hypusination modification of eIF5A[38]. This suggested that ciclopirox has dual antiviral and anti-inflammatory effects. Additionally, previous toxicological studies of ciclopirox have shown that the lethal dose of 50% in mice and rats is 172−83 mg/kg/intraperitoneal and 2500−1700 mg/kg/oral[39]. Recently, a phase I clinical study tested the safety of ciclopirox treatment for hematological malignancies. Dose-limiting toxicities were not observed in hematological patients at 40 mg/m^2 once daily of ciclopirox treatment, which showed that a good toleration of ciclopirox in patients and suggested that ciclopirox has a great potential for human cancer therapy[40]. Combined with preclinical

data of ciclopirox and our animal results that ciclopirox has potent anti-SARS-CoV-2 activity at 20 mg/kg in mice, we believed that ciclopirox might be a safe drug against SARS-CoV-2.

Ciclopirox has been reported to exert anti-cancer activity by inhibiting the expression of multiple iron-dependent enzymes or signaling pathways, such as metalloproteinases[41], ribonucleotide reductase[42], cyclin-dependent kinases[24], Wnt/β-catenin[43] and mTOR signal pathways[44]. Mechanistically, most of these inhibitory effects caused by ciclopirox are attributed to its iron chelating[45-47]. Given this, we performed experiments to examine whether ciclopirox induced NP degradation through its iron chelating. The results suggested that ferrous sulfate ($FeSO_4$) treatment reversed ciclopirox-induced CHK1 degradation, which was consistent with previous reports[48,49]. However, we found that ferrous sulfate treatment did not reverse the level of NP degradation induced by ciclopirox (Supporting Information Fig. S4A). Moreover, ferrous sulfate treatment did not affect the ability that ciclopirox induced NP to form condensates (Fig. S4B). Thus, the mechanism of ciclopirox-induced NP degradation was different from the previous mechanism that ciclopirox inhibited host protein expression as an iron chelator, indicating that it was specific to SARS-CoV-2 NP. Furthermore, the specificity of ciclopirox-induced NP degradation at the virus level was also evaluated. We found that ciclopirox only reduced the expression of NP, but did not affect other structural and non-structural proteins, as well as GFP protein or mCherry protein. This suggested that the ability of ciclopirox to degrade NP is specific at the virus level.

We tried to identify an intermediate protein that mediates the binding of ciclopirox to NP. Liquid chromatography−mass spectrometry (LC−MS) was used to identify differential alterations in host proteins before and after ciclopirox treatment. The LC−MS results showed that 81 host proteins were significantly altered after 5 μmol/L ciclopirox treatment, among which 46 and 35 proteins were up-regulated and down-regulated, respectively. After 20 μmmol/L ciclopirox treatment, 191 differentially expressed proteins were identified, of which 92 proteins were up-regulated and 99 proteins were down-regulated (Fig. S4C). Among these proteins, we selected 19 proteins whose expression was down-regulated after viral infection but up-regulated after ciclopirox treatment at 5 and 20 μmol/L concentrations. In contrast, 19 proteins whose expression was up-regulated after viral infection but down-regulated after treatment with different drugs were also selected (Fig. S4D). Subsequently, we determined whether the expression of these proteins after ciclopirox treatment was consistent with the LC−MS results using Western blotting. The results demonstrated that eight genes could be successfully verified (Fig. S4E). We then assessed the effects of these genes on the expression of NP. Unfortunately, none of these genes affected the expression levels of NP (Data not shown). We next looked for clues from the signaling pathways affected by ciclopirox treatment. The HIF pathway exhibited a high enrichment index after ciclopirox treatment (Fig. S4F). Previous studies have reported that prolyl-hydroxylase (PHD) inhibitors, such as FG-4592 and roxadustat, activate the HIF pathway and then attenuate SARS-CoV-2 replication. One potential antiviral mechanism of PHD inhibitors is interference with ACE2 and TMPRSS2 expression[50,51]. Our RT-qPCR results confirmed that ciclopirox indeed activated HIF pathway indicators, including *HIF1A*, *VEGFA*, *EGLN3*, *NDRG1*, and *CAIX* (Fig. S4G−S4K), but did not affect the mRNA levels of *ACE2* or *TMPRSS2* (Fig. S4L and S4M). Our findings suggested that the antiviral mechanism of ciclopirox was inconsistent with that of PHD inhibitors. Since no relevant hits have been found in the differential expressed proteins or signaling pathways, we speculate that the changes of this intermediate protein during ciclopirox treatment may not be significant, or it may require the joint action of multiple proteins to exert its efficacy, which is a common challenge in the field of drug target identification. As such, this situation significantly increases the complexity and difficulty of hit finding. Given that we have clearly explained the mechanism of ciclopirox specifically induced the NP degradation through the autophagy−lysosomal pathway, we still believe that this is a meaningful and clinically valuable work.

5. Conclusions

Our findings demonstrated that ciclopirox significantly inhibited SARS-CoV-2 replication *in vitro* and *in vivo*. Mechanistically, ciclopirox induced abnormal NP aggregation, and specifically promoted NP degradation in an autophagy−lysosomal manner, resulting in a shorter NP half-life. Further research is needed in the future to find the intermediate protein that mediates the interaction between ciclopirox and NP. Furthermore, due to the relatively high conservation of NP among highly pathogenic coronaviruses, it remained to be determined whether ciclopirox could act as a broad-spectrum inhibitor to disrupt the replication of other coronaviruses such as SARS-CoV, MERS-CoV, and HCoV-OC43. Overall, this study offered a promising drug for controlling the COVID-19 pandemic or potentially future viral pandemics.

Acknowledgments

This work was supported by grants from Shenzhen Science and Technology Program (Grant No. JCYJ20220530163206015, China), National Key Research and Development Program of China (Grant No. 2021YFA0910900), Shenzhen Science and Technology Program (Grant No. JCYJ20220818103017036, China), the National Science Fund for Distinguished Young Scholars (Grant No. 82025022, China), Guangdong Basic and Applied Basic Research Foundation (Grant No. 2023A1515110033, China), Guangdong Science and Technology Plan Project, construction of high-level biosafety laboratories (Grant No. 2021B1212030010, China), Guangdong Basic and Applied Basic Research Foundation (Grant No. 2023A151511 0033, China).

Author contributions

Zheng Zhang and Xiafei Wei conducted and designed the experiments. Xiafei Wei, Yuzheng Zhou, Xiaotong Shen, Lujie Fan, Donglan Liu, Xiang Gao, Jian Zhou, Yezi Wu, Yunfei Li and Wei Feng performed experiments and acquisition of data. Zheng Zhang and Xiafei Wei analyzed and interpreted data. Zheng Zhang and Xiafei Wei wrote the paper and critically reviewed the manuscript.

Conflicts of interest

The authors declare no competing interests.

Appendix A. Supporting information

Supporting data to this article can be found online at https://doi.org/10.1016/j.apsb.2024.03.009.

References

1. World Health Organization. Coronavirus (COVID-19) dashboard. Accessed 14 June 2023. Available from: https://covid19.who.int.
2. Fiolet T, Kherabi Y, MacDonald CJ, Ghosn J, Peiffer-Smadja N. Comparing COVID-19 vaccines for their characteristics, efficacy and effectiveness against SARS-CoV-2 and variants of concern: a narrative review. *Clin Microbiol Infect* 2022;**28**:202−21.
3. Li G, Hilgenfeld R, Whitley R, De Clercq E. Therapeutic strategies for COVID-19: progress and lessons learned. *Nat Rev Drug Discov* 2023;**22**:449−75.
4. Klein EY, Fall A, Norton JM, Eldesouki RE, Abdullah O, Han L, et al. Severity outcomes associated with SARS-CoV-2 XBB variants, an observational analysis. *J Clin Virol* 2023;**165**:105500.
5. Zhang Y, Clarke SP, Wu H, Li W, Zhou C, Lin K, et al. A comprehensive overview on the transmission, pathogenesis, diagnosis, treatment, and prevention of SARS-CoV-2. *J Med Virol* 2023;**95**:e28776.
6. Peng Y, Du N, Lei Y, Dorje S, Qi J, Luo T, et al. Structures of the SARS-CoV-2 nucleocapsid and their perspectives for drug design. *EMBO J* 2020;**39**:e105938.
7. Zhao H, Wu D, Hassan SA, Nguyen A, Chen J, Piszczek G, et al. A conserved oligomerization domain in the disordered linker of coronavirus nucleocapsid proteins. *Sci Adv* 2023;**9**:eadg6473.
8. Scherer KM, Mascheroni L, Carnell GW, Wunderlich LCS, Makarchuk S, Brockhoff M, et al. SARS-CoV-2 nucleocapsid protein adheres to replication organelles before viral assembly at the Golgi/ERGIC and lysosome-mediated egress. *Sci Adv* 2022;**8**:eabl4895.
9. Kang S, Yang M, Hong Z, Zhang L, Huang Z, Chen X, et al. Crystal structure of SARS-CoV-2 nucleocapsid protein RNA binding domain reveals potential unique drug targeting sites. *Acta Pharm Sin B* 2020;**10**:1228−38.
10. Wang W, Chen J, Yu X, Lan HY. Signaling mechanisms of SARS-CoV-2 nucleocapsid protein in viral infection, cell death and inflammation. *Int J Biol Sci* 2022;**18**:4704−13.
11. Zhao Y, Sui L, Wu P, Wang W, Wang Z, Yu Y, et al. A dual-role of SARS-CoV-2 nucleocapsid protein in regulating innate immune response. *Signal Transduct Target Ther* 2021;**6**:331.
12. Netea MG, Ziogas A, Benn CS, Giamarellos-Bourboulis EJ, Joosten LAB, Arditi M, et al. The role of trained immunity in COVID-19: lessons for the next pandemic. *Cell Host Microbe* 2023;**31**:890−901.
13. Wang S, Dai T, Qin Z, Pan T, Chu F, Lou L, et al. Targeting liquid−liquid phase separation of SARS-CoV-2 nucleocapsid protein promotes innate antiviral immunity by elevating MAVS activity. *Nat Cell Biol* 2021;**23**:718−32.
14. Royster A, Ren S, Ma Y, Pintado M, Kahng E, Rowan S, et al. SARS-CoV-2 nucleocapsid protein is a potential therapeutic target for anti-coronavirus drug discovery. *Microbiol Spectr* 2023;**11**:e0118623.
15. Hu X, Zhou Z, Li F, Xiao Y, Wang Z, Xu J, et al. The study of antiviral drugs targeting SARS-CoV-2 nucleocapsid and spike proteins through large-scale compound repurposing. *Heliyon* 2021;**7**:e06387.
16. Wang YT, Long XY, Ding X, Fan SR, Cai JY, Yang BJ, et al. Novel nucleocapsid protein-targeting phenanthridine inhibitors of SARS-CoV-2. *Eur J Med Chem* 2022;**227**:113966.
17. Wu Y, Ma L, Cai S, Zhuang Z, Zhao Z, Jin S, et al. RNA-induced liquid phase separation of SARS-CoV-2 nucleocapsid protein facilitates NF-κB hyper-activation and inflammation. *Signal Transduct Target Ther* 2021;**6**:167.
18. Zhao M, Yu Y, Sun LM, Xing JQ, Li T, Zhu Y, et al. GCG inhibits SARS-CoV-2 replication by disrupting the liquid phase condensation of its nucleocapsid protein. *Nat Commun* 2021;**12**:2114.
19. Zhao D, Xu W, Zhang X, Wang X, Ge Y, Yuan E, et al. Understanding the phase separation characteristics of nucleocapsid protein provides a new therapeutic opportunity against SARS-CoV-2. *Protein Cell* 2021;**12**:734−40.
20. Yaron TM, Heaton BE, Levy TM, Johnson JL, Jordan TX, Cohen BM, et al. The FDA-approved drug alectinib compromises SARS-CoV-2 nucleocapsid phosphorylation and inhibits viral infection *in vitro*. *bioRxiv* 2020. Available from: https://doi.org/10.1101/2020.08.14.251207.
21. Liu X, Verma A, Garcia Jr G, Ramage H, Lucas A, Myers RL, et al. Targeting the coronavirus nucleocapsid protein through GSK-3 inhibition. *Proc Natl Acad Sci U S A* 2021;**118**:e2113401118.
22. Cubuk J, Alston JJ, Incicco JJ, Singh S, Stuchell-Brereton MD, Ward MD, et al. The SARS-CoV-2 nucleocapsid protein is dynamic, disordered, and phase separates with RNA. *Nat Commun* 2021;**12**:1936.
23. Evaluation of a new antifungal cream, ciclopirox olamine 1% in the treatment of cutaneous candidosis. *Clin Ther* 1985;**8**:41−8.
24. Zhou H, Shen T, Luo Y, Liu L, Chen W, Xu B, et al. The antitumor activity of the fungicide ciclopirox. *Int J Cancer* 2010;**127**:2467−77.
25. Zangi M, Donald KA, Casals AG, Franson AD, Yu AJ, Marker EM, et al. Synthetic derivatives of the antifungal drug ciclopirox are active against herpes simplex virus 2. *Eur J Med Chem* 2022;**238**:114443.
26. Bernier KM, Morrison LA. Antifungal drug ciclopirox olamine reduces HSV-1 replication and disease in mice. *Antiviral Res* 2018;**156**:102−6.
27. Caceres CJ, Angulo J, Contreras N, Pino K, Vera-Otarola J, Lopez-Lastra M. Targeting deoxyhypusine hydroxylase activity impairs cap-independent translation initiation driven by the 5′untranslated region of the HIV-1, HTLV-1, and MMTV mRNAs. *Antiviral Res* 2016;**134**:192−206.
28. Hoque M, Hanauske-Abel HM, Palumbo P, Saxena D, D'Alliessi Gandolfi D, Park MH, et al. Inhibition of HIV-1 gene expression by ciclopirox and deferiprone, drugs that prevent hypusination of eukaryotic initiation factor 5A. *Retrovirology* 2009;**6**:90.
29. Kang JA, Kim S, Park M, Park HJ, Kim JH, Park S, et al. Ciclopirox inhibits hepatitis B virus secretion by blocking capsid assembly. *Nat Commun* 2019;**10**:2184.
30. Li A, Yang DH. Application of immunohistochemistry in basic and clinical studies. *Methods Mol Biol* 2020;**2108**:43−55.
31. Martinez Molina D, Jafari R, Ignatushchenko M, Seki T, Larsson EA, Dan C, et al. Monitoring drug target engagement in cells and tissues using the cellular thermal shift assay. *Science* 2013;**341**:84−7.
32. Chen H, Cui Y, Han X, Hu W, Sun M, Zhang Y, et al. Liquid−liquid phase separation by SARS-CoV-2 nucleocapsid protein and RNA. *Cell Res* 2020;**30**:1143−5.
33. Hipp MS, Park SH, Hartl FU. Proteostasis impairment in protein-misfolding and -aggregation diseases. *Trends Cell Biol* 2014;**24**:506−14.
34. Sturner E, Behl C. The role of the multifunctional BAG3 protein in cellular protein quality control and in disease. *Front Mol Neurosci* 2017;**10**:177.
35. Wang X, Luo J, Wen Z, Shuai L, Wang C, Zhong G, et al. Diltiazem inhibits SARS-CoV-2 cell attachment and internalization and decreases the viral infection in mouse lung. *PLoS Pathog* 2022;**18**:e1010343.
36. Pan P, Shen M, Yu Z, Ge W, Chen K, Tian M, et al. SARS-CoV-2 N protein promotes NLRP3 inflammasome activation to induce hyperinflammation. *Nat Commun* 2021;**12**:4664.
37. Liang S, Yang Z, Hua L, Chen Y, Zhou Y, Ou Y, et al. Ciclopirox inhibits NLRP3 inflammasome activation *via* protecting mitochondria and ameliorates imiquimod-induced psoriatic inflammation in mice. *Eur J Pharmacol* 2022;**930**:175156.
38. Anderson-Baucum E, Pineros AR, Kulkarni A, Webb-Robertson BJ, Maier B, Anderson RM, et al. Deoxyhypusine synthase promotes a pro-inflammatory macrophage phenotype. *Cell Metab* 2021;**33**:1883−1893.e7.
39. Weir SJ, Patton L, Castle K, Rajewski L, Kasper J, Schimmer AD. The repositioning of the anti-fungal agent ciclopirox olamine as a novel therapeutic agent for the treatment of haematologic malignancy. *J Clin Pharm Ther* 2011;**36**:128−34.
40. Minden MD, Hogge DE, Weir SJ, Kasper J, Webster DA, Patton L, et al. Oral ciclopirox olamine displays biological activity in a phase I study in patients with advanced hematologic malignancies. *Am J Hematol* 2014;**89**:363−8.
41. Qi J, Zhou N, Li L, Mo S, Zhou Y, Deng Y, et al. Ciclopirox activates PERK-dependent endoplasmic reticulum stress to drive cell death in colorectal cancer. *Cell Death Dis* 2020;**11**:582.

42. Greene BL, Kang G, Cui C, Bennati M, Nocera DG, Drennan CL, et al. Ribonucleotide reductases: structure, chemistry, and metabolism suggest new therapeutic targets. *Annu Rev Biochem* 2020;**89**:45−75.
43. Kim Y, Schmidt M, Endo T, Lu D, Carson D, Schmidt-Wolf IG. Targeting the Wnt/beta-catenin pathway with the antifungal agent ciclopirox olamine in a murine myeloma model. *In Vivo* 2011;**25**: 887−93.
44. Zhou H, Shang C, Wang M, Shen T, Kong L, Yu C, et al. Ciclopirox olamine inhibits mTORC1 signaling by activation of AMPK. *Biochem Pharmacol* 2016;**116**:39−50.
45. Eberhard Y, McDermott SP, Wang X, Gronda M, Venugopal A, Wood TE, et al. Chelation of intracellular iron with the antifungal agent ciclopirox olamine induces cell death in leukemia and myeloma cells. *Blood* 2009;**114**:3064−73.
46. Shen T, Huang S. Repositioning the old fungicide ciclopirox for new medical uses. *Curr Pharm Des* 2016;**22**:4443−50.
47. Huang Z, Huang S. Reposition of the fungicide ciclopirox for cancer treatment. *Recent Pat Anti-Cancer Drug Discov* 2021;**16**:122−35.
48. Shen T, Shang C, Zhou H, Luo Y, Barzegar M, Odaka Y, et al. Ciclopirox inhibits cancer cell proliferation by suppression of Cdc25A. *Genes Cancer* 2017;**8**:505−16.
49. Malumbres M, Barbacid M. Cell cycle, CDKs and cancer: a changing paradigm. *Nat Rev Cancer* 2009;**9**:153−66.
50. Wing PAC, Prange-Barczynska M, Cross A, Crotta S, Orbegozo Rubio C, Cheng X, et al. Hypoxia inducible factors regulate infectious SARS-CoV-2, epithelial damage and respiratory symptoms in a hamster COVID-19 model. *PLoS Pathog* 2022;**18**: e1010807.
51. Wing PAC, Keeley TP, Zhuang X, Lee JY, Prange-Barczynska M, Tsukuda S, et al. Hypoxic and pharmacological activation of HIF inhibits SARS-CoV-2 infection of lung epithelial cells. *Cell Rep* 2021; **35**:109020.